ARCHIVES
of
FOUNDRY ENGINEERING

ISSN (2299-2944)
Volume 2025
Issue 3/2025

221 – 226

10.24425/afe.2025.155371

25/3

Published quarterly as the organ of the Foundry Commission of the Polish Academy of Sciences

Improving Cavitation Wear Resistance of Cast Iron Valve Castings by Applying Austenitic Steel Overlays

M. Jacek-Burek*, M. Mróz
Rzeszow University of Technology, Al. Powstańców Warszawy 12, 35-959 Rzeszów, Poland
* Corresponding author. e-mail address: m.jacek@prz.edu.pl

Received 15.07.2025; accepted in revised form 29.08.2025; available online 19.09.2025

Abstract

This study presents the results of cavitation wear resistance tests of AISI 307 and AISI 316 steel overlays. The overlays were applied using plasma cladding. The cladding was performed on spheroidal graphite cast iron castings with a ferritic-pearlitic matrix. The cavitation wear process was analyzed based on surface topography measurements, focusing on the S_z parameter, defined as the height difference between the highest peak and the deepest valley on the surface. Additionally, surface condition after cavitation exposure was examined using scanning electron microscopy. The material currently used for valve components, i.e. cast iron, exhibits significantly lower cavitation resistance compared to the overlays made of AISI 307 and AISI 316 stainless steels. The application of plasma cladding to produce surface overlays significantly increases the service life of cast iron valve components exposed to hydraulic impact, particularly in environments where cavitation-induced degradation occurs.

Keywords: Spheroidal graphite cast iron castings, Plasma surfacing, Cavitation, Surface topography

1. Introduction

Maintaining stable water pressure in extensive systems such as water supply networks is challenging due to the potential occurrence of water hammer. Water hammer manifests as strong pressure oscillations in water pipelines, caused by rapid changes in flow velocity that affect the inertia of the water mass moving through the pipeline. A sudden change in water flow velocity and the resulting change in flow volume leads to a redistribution of kinetic and potential energy within the cross-section of the pipeline, causing an increase or decrease in water pressure. Water hammer may result from random events such as power outages or equipment failures, improper network operation, or cavitation induced by excessive water flow velocity [1–3].

Cavitation may occur in all systems and configurations that transport fluids (flow machines, water supply networks, cooling systems) where significant velocity distribution heterogeneity exists [4]. When the flow velocity of a liquid increases rapidly, the static pressure and the boiling temperature of the liquid decrease. At a critical pressure, the liquid begins to boil, forming gas bubbles filled with water vapor or dissolved gases, which collapse rapidly under elevated pressure due to implosion.

Implosion of the bubbles generates spherical shock waves. If the center of implosion is located at a distance from the metal surface equal to the radius of the collapsing bubble, the pressure of the shock wave may exceed the material yield strength, resulting in crater-shaped damage [5–6].

Surface degradation due to cavitation is particularly significant in cast iron fittings such as valve bodies and gate valves, especially in areas where high sealing performance is required. As noted in

studies [7–9], one method of improving resistance to cavitation wear is surface layer modification of the casting through cladding.

The aim of this study is to demonstrate the potential for improving cavitation resistance of ferritic-pearlitic spheroidal graphite cast iron by applying AISI 307 and AISI 316 steel overlays.

2. Materials and Methods

The cladding was applied to spheroidal graphite cast iron castings with a ferritic-pearlitic matrix. A representative microstructure of the base material is shown in Figure 1.

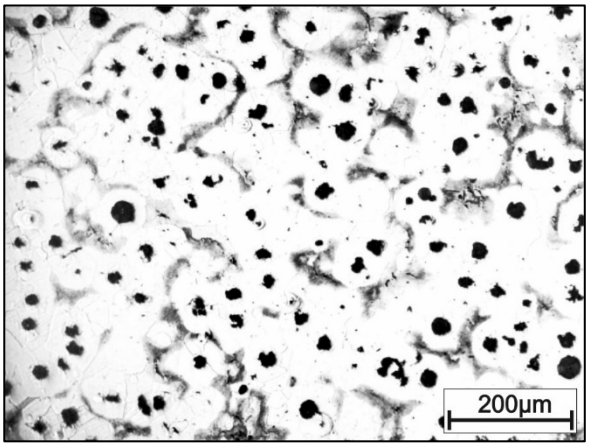

Fig. 1. Microstructure of spheroidal graphite cast iron – substrate for cladding. Nital-etched specimen. Magnification 100x

The chemical composition of the cast iron is presented in Table 1.

Table 1.
Results of chemical composition analysis of the cast iron

Element content, wt.%								
C	**Si**	**Mn**	**P**	**S**	**Ni**	**Cu**	**Mg**	**Fe**
3.43	2.5	0.1	0.01	0.01	0.02	0.01	0.05	balance

The AISI 316 and AISI 307 austenitic steel overlays were applied using plasma cladding. AISI 307 and AISI 316 powders were used for the overlays. SEM images and the chemical composition of the powders are shown in Figures 2 and 3.

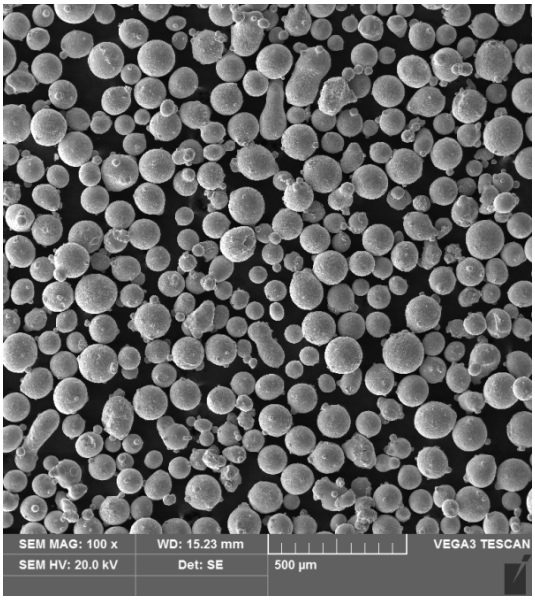

Fe	Cr	Ni	Mn	Si
63.67	22.54	7.15	5.7	0.94

Fig.2. Image of AISI 307 powder particles with chemical composition, wt.%

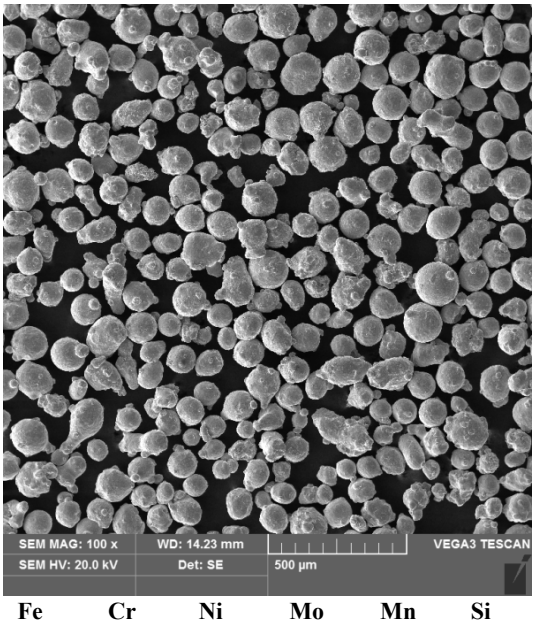

Fe	Cr	Ni	Mo	Mn	Si
63.3	18.9	10.9	2.82	0.69	1.21

Fig.3. Image of AISI 316 powder particles with chemical composition, wt.%

The plasma cladding process was performed using the GAP 2501 DC device torch and a Comau MTR Syn 5 robot.

The technological parameters used for applying the AISI 307 and AISI 316 overlays via plasma cladding are listed in Table 2.

Table 2.
Technological parameters of the plasma cladding process for AISI 307 and AISI 316 steel overlays

Current intensity	120 A
Electric arc voltage	23.5 V
Electrode type / diameter	W/4 mm
Plasma gas (argon)	1 l/min
Shielding gas (argon)	7 l/min
Powder feed rate	20%
Powder carrier gas (argon)	2 l/min
Torch travel speed	16 mm/min

Cavitation wear resistance tests were carried out on metallographic specimens prepared from samples cut from the cast iron substrate and from the AISI 307 and AISI 316 steel overlays. The tests were conducted using a Vibra-Cell Sonics device equipped with a head containing a piezoelectric transducer operating at a vibration frequency of 20 kHz. The test samples were placed at a distance of 0.5 mm from the transducer head. Tap water from the water supply network was used during testing. The cavitation exposure time was 120 minutes.

After the cavitation erosion test, the degree of surface degradation, defined as the depth of cavitation damage, was assessed. Surface topography of the samples was evaluated both before and after the cavitation erosion test using a T8000 profilometer from Hommel Etamic, equipped with Hommel Map Expert 6.2 software. The analyzed area of the sample, where cavitation acted, was square-shaped with sides of 8 mm. The S_z parameter of the surface topography, representing the height difference between the highest peak and the deepest valley, was measured. Surface observations of the samples were also performed using a Vega 3 scanning electron microscope from Tescan.

3. Results and Analysis

Representative microstructures and chemical compositions of the AISI 307 and AISI 316 steel overlays are presented in Figures 4 and 5. The deposited layer height of the weld overlay produced from AISI 307 steel was 2.26 mm, while that of the weld overlay produced from AISI 316 steel was 2.41 mm.

The results of SEM observations and chemical composition analysis indicate that the AISI 307 overlay consists of γ-nickel austenite grains rich in iron, chromium, nickel, and manganese, with the presence of silicon, and eutectic structures (γ-austenite + carbides) located along the grain boundaries. The carbides in this eutectic are rich in chromium and iron. The AISI 316 overlay also consists of γ-nickel austenite grains rich in iron, chromium, nickel, and manganese, with the presence of silicon, and eutectic structures (γ-austenite + carbides) at the grain boundaries. The carbides are rich in chromium and iron and also contain molybdenum and manganese.

Representative 2D surface profilograms of the initial state (prior to cavitation) for the spheroidal cast iron sample and the overlays are shown in Figure 6. All sample surfaces were characterized by similar values of the S_z surface texture parameter.

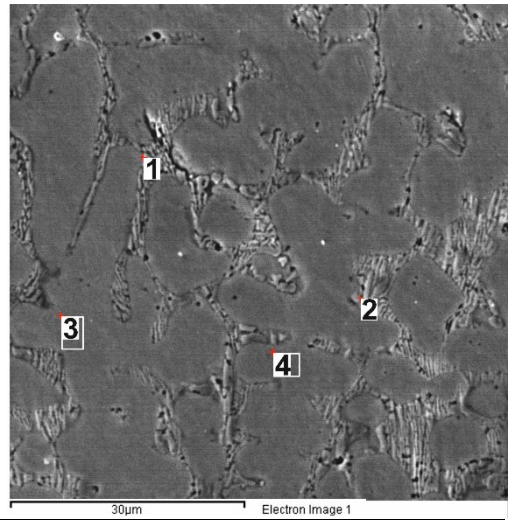

Point	C	Si	Cr	Mn	Ni	Fe
1	6.60	1.38	17.60	4.31	3.25	66.83
2	6.66	1.71	14.11	4.49	3.66	69.37
3	2.99	1.53	8.82	3.08	5.09	78.49
4	2.52	1.69	8.74	3.00	5.38	78.66

Fig. 4. Microstructure and chemical composition of the AISI 307 weld overlay, wt.%

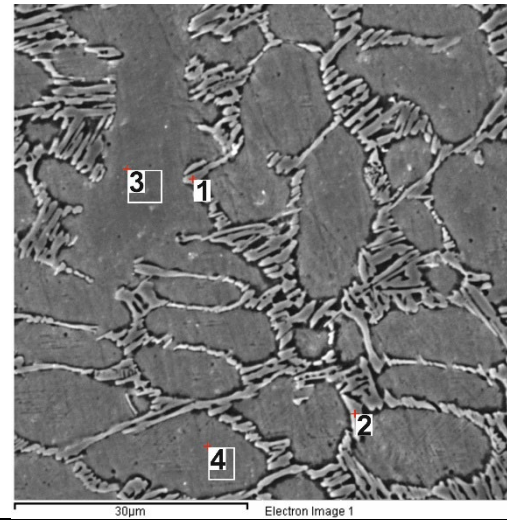

Point	C	Si	Cr	Mn	Mo	Ni	Fe
1	9.56	0.45	16.59	1.07	2.06	1.41	68.85
2	8.82	0.36	16.00	1.06	1.75	1.43	70.59
3	2.51	2.10	5.61	0.45	0.00	5.89	83.43
4	3.07	2.03	5.03	0.55	0.00	5.48	83.83

Fig. 5. Microstructure and chemical composition of the AISI 316 weld overlay, wt.%

Representative surface views of the cast iron substrate sample and the surfaces of the AISI 307 and AISI 316 weld overlays after cavitation wear resistance testing (after 120 minutes) are shown in Figures 7–9.

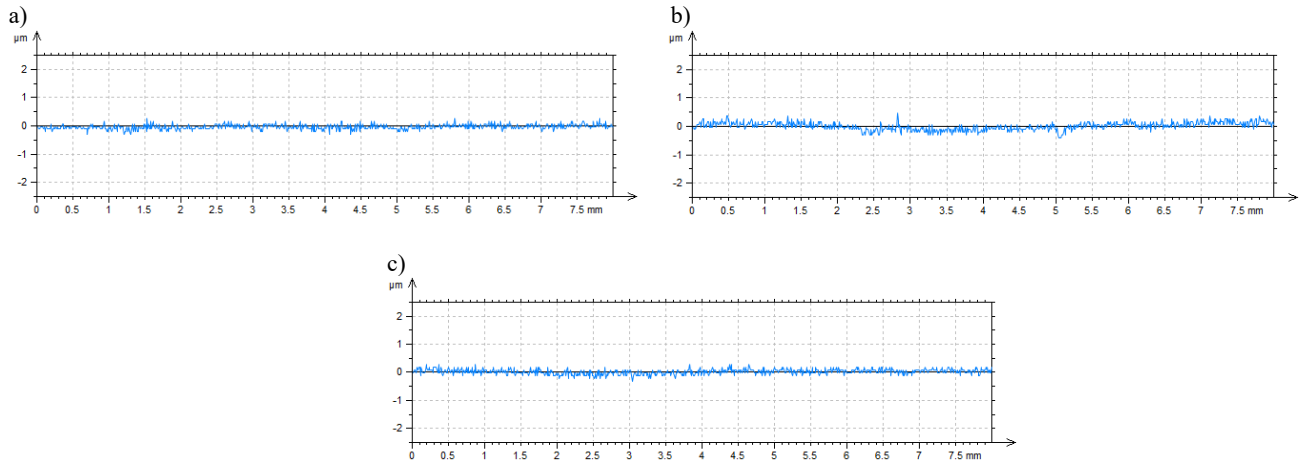

Fig. 6. Representative surface profilograms in the initial condition: a) spheroidal cast iron sample with a ferritic-pearlitic matrix, b) AISI 307 weld overlay, c) AISI 316 weld overlay

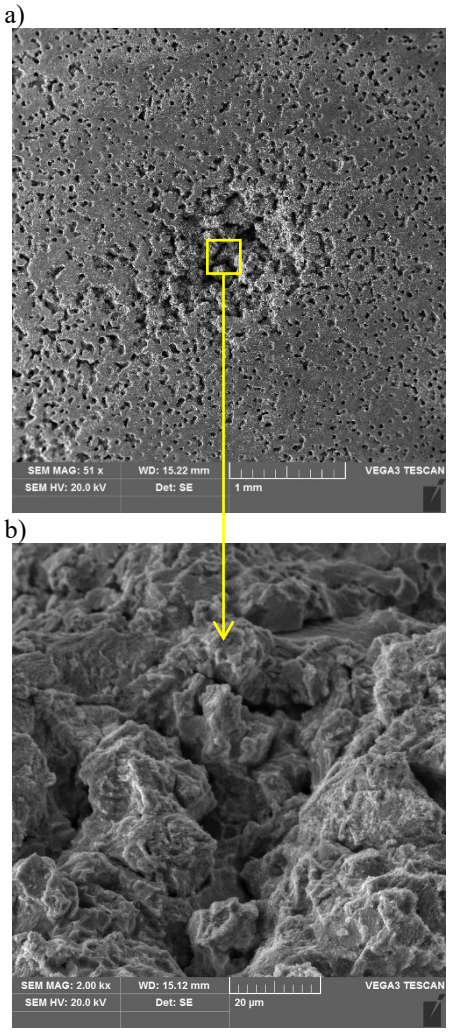

Fig. 7. Representative surface view of the cast iron substrate sample after cavitation wear resistance testing

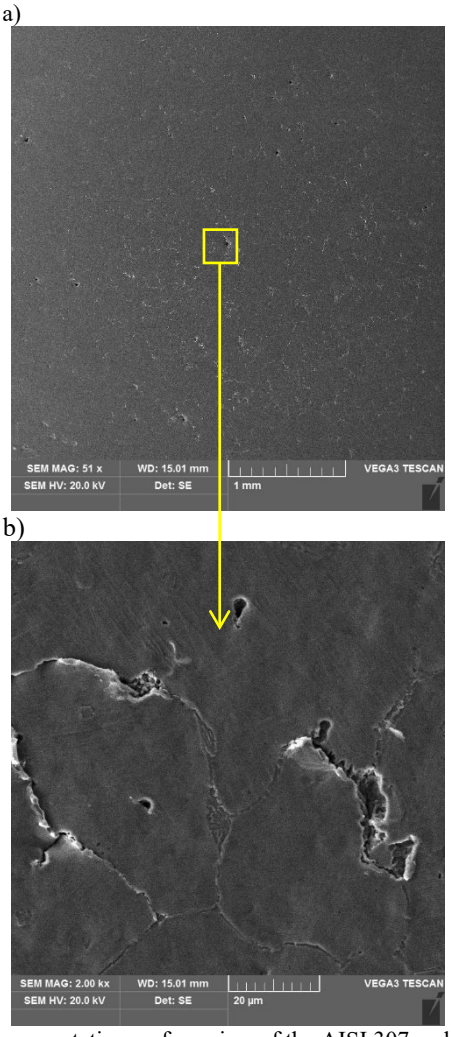

Fig. 8. Representative surface view of the AISI 307 weld overlay after cavitation wear resistance testing

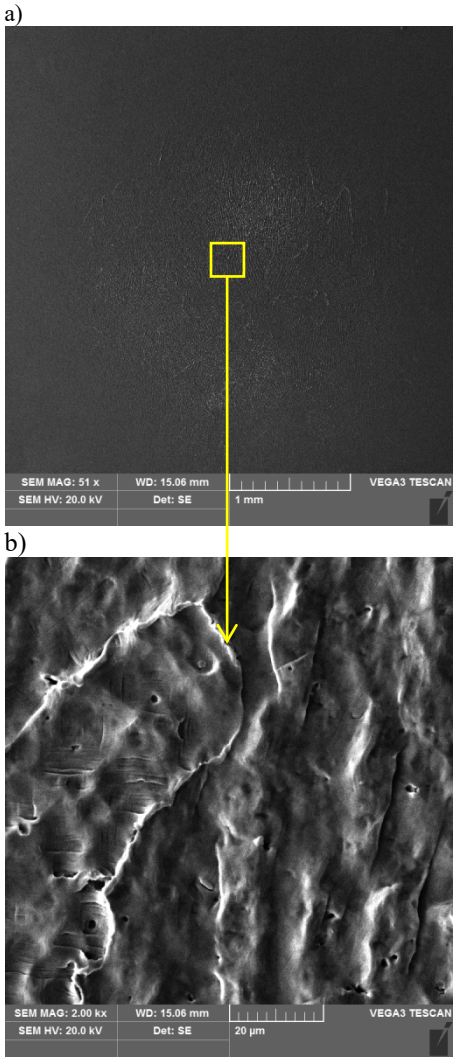

Fig. 9. Representative surface view of the AISI 316 weld overlay after cavitation wear resistance testing

Analysis of profilograms taken across the central zone affected by cavitation reveals significantly greater cavitation pit depths in the cast iron sample compared to the surface of samples with AISI 307 and AISI 316 weld overlays. This is reflected in the values of the S_z surface texture parameter.

3D maps and example profilograms passing through the central area of cavitation impact on the samples made of cast iron substrate as well as on the samples with AISI 307 and AISI 316 overlays are presented in Figures 10–12.

The results of surface topography parameter S_z measurements in the central cavitation impact area on the cast iron substrate samples and on the samples with AISI 307 and AISI 316 overlays are presented in Table 3.

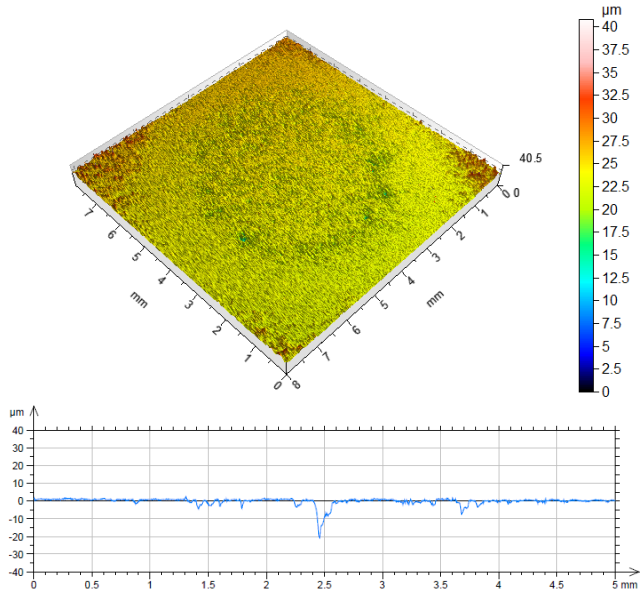

Fig. 10. Example 3D map and profilogram in the central area of cavitation impact on the surface of the cast iron substrate sample

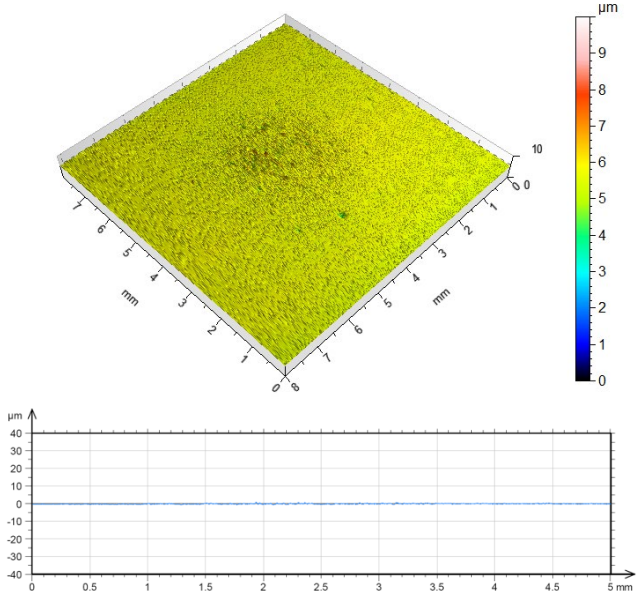

Fig. 11. Example 3D map and profilogram in the central area of cavitation impact on the surface of the AISI 307 steel overlay

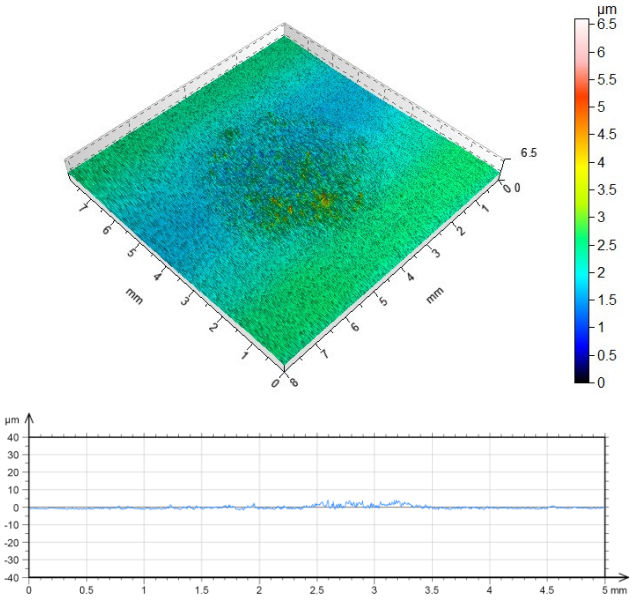

Fig. 12. Example 3D map and profilogram in the central area of cavitation impact on the surface of the AISI 316 steel overlay

Table 3.
S_z surface topography parameter values in the central area of cavitation impact

Material	S_z value, µm	
	initial state	post-cavitation
cast iron	0.60	20.6
AISI 307 steel overlay	0.70	1.20
AISI 316 steel overlay	0.70	4.50

The obtained test results indicate that the highest degree of surface degradation due to cavitation occurred in the cast iron samples. In contrast, the degradation level of the surfaces with AISI 307 and AISI 316 overlays was significantly lower. This finding was confirmed by the measured values of the S_z surface topography parameter, with the ductile iron sample showing a much higher S_z value compared to the overlays.

4. Conclusions

Based on the obtained results, the following conclusions can be drawn:

- The material currently used for valve components, i.e. cast iron, exhibits significantly lower cavitation resistance compared to the overlays made of AISI 307 and AISI 316 stainless steels.
- The application of plasma cladding to produce surface overlays significantly increases the service life of cast iron valve components exposed to hydraulic impact, particularly in environments where cavitation-induced degradation occurs.

References

[1] Niełacny M. (2023). *Water hammer in water supply systems*. Poznań: Publishing House of Poznań University of Technology (in Polish).

[2] Malesińska, A. (2014). Water hammer – why it occurs and haw to prevent it. *Instal Reporter.* 3, 38-41. (in Polish).

[3] Bonetyński, K. & Wiszniewska-Oraczewska, I. (2001). Strategy for protection against the adverse effects of water hammer in water supply networks. *Gaz, Water and Sanitation*. 8, 283-286. (in Polish).

[4] Szkodko, M. (2008). *Cavitation erosion of metal construction materials. Monografia*. Gdańsk: Publishing House of Gdańsk University of Technology. (in Polish)

[5] Stachowiak, G. W., & Batchelor, A. W. (1993). Abrasive, erosive and cavitation wear. In *Engineering tribology* (pp. 501–551). Oxford: Butterworth-Heinemann.

[6] Dudziak, A. (2013). Cavitation – advantages and disadvantages. Retrieved March 18, 2025, from http://www.instalator.pl/2013/12/kawiatacja-zalety-i-wady-dynamiczne-pecherzyki. (in Polish)

[7] Adamski. M. (2009). Cavitation - a neglected phenomenon. *Energy*. 46-49. (in Polish).

[8] Arrojo, S., Benito, Y. (2008). A theoretical study of hydrodynamic cavitation. *Ultrasonics Sonochemistry.* 15(3), 203-211. https://doi.org/10.1016/j.ultsonch.2007.03.007.

[9] Lenik, K. & Ozonek, J. (2012). Possibility of estimating the number of cavitation in hydrodynamic cavitation processes, taking into account the influence of the cavitation inductor geometry. *Measurements Automation Robotics*. 6, 60-66. (in Polish).